Neptunium redox speciation at the illite surface

Rémi Marsac, Nidhu lal Banik [*], Johannes Lützenkirchen,
Christian Michael Marquardt, Kathy Dardenne, Dieter Schild, Joerg Rothe,
Alexandre Diascorn, Tomas Kupcik, Thorsten Schäfer, Horst Geckeis

Institut für Nukleare Entsorgung, Karlsruhe Institute of Technology, P.O. Box 3640, D 76021 Karlsruhe, Germany

Abstract

Neptunium (Np(V)) sorption onto a purified illite is investigated as a function of pH (3 10) and $[Np^{V}O_2^+]_{tot}(3 \times 10^{-8}$ 3×10^{-4} M) in 0.1 M NaCl under Ar atmosphere. After about one week reaction time, only insignificant variation of Np sorption is observed and the establishment of reaction equilibrium can be assumed. Surprisingly, solid liquid distribution ratios (R_d) are clearly higher than those measured for Np(V) sorption onto illite under aerobic conditions. The observation that R_d increases with decreasing pe (pe = log a_{e-}) suggests partial reduction to Np(IV), although measured redox potentials (pe values) at a first glance suggest the predominance of Np(V). Reduction to Np(IV) at the illite surface could indeed be confirmed by X ray absorption near edge spectroscopy (XANES). Np speciation in presence of the purified Na illite under given conditions is consistently described by applying the 2 sites protolysis non electrostatic surface complexation and cation exchange model. Measured pe data are taken to calculate Np redox state and surface complexation constants for Np(IV) are derived by applying a data fitting procedure. Constants are very consistent with results obtained by applying an existing linear free energy relationship (LFER). Taking Np(IV) surface complexation constants into account shifts the calculated Np(V)/Np(IV) redox borderline in presence of illite surfaces by 3 5 pe units (0.2 0.3 V) towards redox neutral conditions. Our study suggests that Np(V) reduction in presence of a sorbing mineral phase is thermodynamically favored.

1. INTRODUCTION

Neptunium (Np) is only a minor constituent of high level radioactive waste. Its environmental chemistry is still of considerable interest due to the long half life of its main isotope ^{237}Np ($t_{1/2} = 2 \times 10^6$ a) and its high solubility and mobility as pentavalent $Np(V)O_2^+$ under oxidizing conditions. In general, Np can exist in oxidation states between +III and +VII in aqueous solution, but penta and tetravalent Np are the most relevant oxidation states in the geosphere (Kim, 1986). NpO_2^+ only weakly sorbs to mineral surfaces and is therefore regarded as rather mobile (Geckeis et al., 2013). Under reducing conditions, Np(IV) prevails and is considered as rather immobile because of its strong sorption to minerals and due to its low solubility, as other tetravalent actinides (An; e.g. Th(IV)) or other tetravalent elements (e.g. Sn(IV)) (Bradbury and Baeyens, 2009a,b).

Clay minerals are main components in sedimentary rocks, which are considered as potential host rocks for radioactive waste disposal (e.g. Callovo Oxfordian mudstone, France; Opalinus Clay) (Claret et al., 2005; Latrille et al., 2006; Wu et al., 2009). Their high sorption capacity for cations via ion exchange reactions as well as surface

---

[*] Corresponding author. Tel.: +49 72160822420; fax: +49 72160823927.

E mail address: nidhu.banik@kit.edu (N.l. Banik).

complexation to silanol or aluminol groups at the edge of clay particles have a major impact on radionuclide and metal ion retention. Np sorption onto purified clay minerals has mostly been studied under aerobic conditions, where the +V oxidation state is dominant or under inert atmosphere but without monitoring or controlling the redox potential (Gorgeon, 1994; Turner et al., 1998; Amayri et al., 2011). As slightly reducing conditions are frequently found in soil or natural clay rocks, it is mandatory to assess the impact of redox conditions on the behavior of redox active metal ions such as Np. Partial reduction of Np(V) to Np(IV) when in contact with Opalinus Clay was suggested by comparing sorption data obtained under aerobic and anaerobic conditions. Stronger Np sorption (Fröhlich et al., 2011) was found under anaerobic conditions and significant reduction to Np(IV) was evidenced by applying synchrotron based spectroscopic techniques (Fröhlich et al., 2012). Np(IV) was found associated with pyrite as the main reductant in the natural clay rock.

The oxidation state of the early actinides (Pa, U, Np, Pu) is determined by the redox potential in solution, which in turn is controlled by the balance of redox pairs (see e.g. Altmaier et al., 2013). Establishment of redox equilibria in homogeneous solution may however be slow. For instance, Nakata et al. (2002) observed almost no Np(V) reduction by dissolved Fe(II) after one week. By contrast, reactions with redox active solid phases are usually found to proceed fast (Stumm, 1992; Buerge and Hug, 1999; Liger et al., 1999; Nakata et al., 2002; Charlet et al., 2007; Bach et al., 2014). Notably for reactions with Pu(V) with mineral surfaces rapid reduction to Pu(IV) is stated (Powell et al., 2004, 2005; Hixon et al., 2010; Kirsch et al., 2011; Zaravin et al., 2012). The time necessary for a complete Pu(V) reduction varies from few hours to few days depending on the mineral. Spectroscopic and microscopic examination very often reveal that reduced Pu(IV) species are predominantly found at the mineral surface, thus implying surface mediated reduction being the relevant reaction mechanism. Reduction is, however, also found at mineral surfaces where a specific reducing partner is absent (Hixon et al., 2013), suggesting that Pu(IV) under given conditions simply is the thermodynamically favored species. Zaravin et al. (2012) studied Np(V) sorption onto montmorillonite under the same conditions as for Pu(V), but did not observe Np(V) reduction. This observation can be explained by the fact that the standard redox potential of the Np(V)/Np(IV) couple ($E^0_{NpO_2^+/Np^{4+}} = 0.604$ V) is lower than that of the Pu(V)/Pu(IV) pair $E_{PuO_2^+/Pu^{4+}} = 1.031$ V (Guillaumont et al., 2003). Therefore, reduction of Np(V) to Np(IV) in presence of montmorillonite surfaces under given conditions apparently is not thermodynamically favorable.

Only a few attempts are reported in the literature to describe actinide redox reactions in presence of minerals quantitatively by applying mechanistic surface complexation models. Such thermodynamic models are particularly relevant and required for a comprehensive prediction of actinide behavior in natural systems. Degueldre and Bolek (2009) discussed Pu sorption to Al_2O_3, FeOOH and SiO_2 colloids based on a simple R_d approach. Their calculations included the effect of the redox potential, which was shown to have a major impact on calculated Pu uptake data. Schwantes and Santschi (2010) proposed a surface complexation model involving all Pu redox states (from +III to +VI) to minerals and a reversible surface mediated Pu(V) Pu(IV) reaction to explain the observed kinetics of Pu uptake. Experimentally determined redox potential (pe; Eh) or $O_{2(g)}$ partial pressures are essential for the application of surface complexation models to describe sorption behavior of redox sensitive elements. However, in most studies mentioned above, such data are not provided, very often due to difficulties associated with their experimental determination (Schüring et al., 2000; Altmaier et al., 2010).

The present study is dedicated to NpO_2^+ sorption to a purified clay mineral (illite) under inert gas atmosphere (Argon) in order to exclude the influence of atmospheric CO_2. Classical batch experiments at various pH, total Np concentrations and reaction times are performed and compared with literature data for the uptake of various metal ions onto illite. Different to many other similar studies a special focus is dedicated to monitor redox conditions. X ray absorption near edge structure spectroscopy (XANES) is applied to determine the Np redox state at the illite surface. Finally, an attempt is made to consistently describe Np sorption and redox speciation using surface complexation modeling.

2. MATERIALS AND METHODS

All chemicals are of pro analytical quality or better and were obtained from Merck (Darmstadt, Germany) or Riedel de Haen (Seelze, Germany). All experiments were conducted with de ionized “MilliQ” water (specific resistivity, 18.2 MΩ cm^{-1}). The aqueous concentration of ^{237}Np was analyzed using LSC with a TriCarb 3100 (Beckman/PerkinElmer) and the scintillation cocktail Ultima Gold XR (Packard Instruments Co., USA). To differentiate between the alpha decay of the ^{237}Np and the beta decay of its daughter ^{233}Pa, the measurements have been performed in an alpha beta discrimination mode applying a Pulse Decay Analysis (PDA), a form of pulse shape analysis, to perform differentiation of alpha and beta events. PDA uses a time based Pulse Decay Discriminator (PDD) to evaluate the pulse duration of scintillation events and categorize the events as either alpha or beta. A discriminator (146) setting was used to reduce the beta spillover to 1.50%. ^{237}Np counting efficiencies for each sample were determined using a ^{237}Np quenching curve. Each sample was counted for a total of 0.5 h. Since we used a constant background electrolyte (0.1 M NaCl), the Quench Indicating Parameter (QIP) tSIE fixed to 470 does not change significantly (±10) during the LSC measurements. Details about the LSC measurement are given in the supplementary information. In addition, the stock solution of ^{237}Np and aqueous concentration of ^{237}Np in the batch sorption experiment after phase separation were also checked at random by ICP MS measurements and the results are in good agreement with LSC measurements.

2.1. Neptunium stock solution

The initial ^{237}Np solution was evaporated to dryness and dissolved in 8 M HCl. The solution was purified via anion exchange (BIO RAD® AG 1 X8). After a washing step with several milliliters of 8 M HCl, Pu contaminations were removed with a fresh solution of 150 mg NH_4I in 5 mL 8 M HCl. Subsequently, Np was eluted from the ion exchanger with 4 M HCl/0.05 M HF and evaporated to dryness in a PTFE beaker. For all sorption experiments, stock solutions of neptunium in the pentavalent oxidation state were to be used. To obtain a solution containing only NpO_2^+, the solution was fumed twice with 1 M $HClO_4$ and the residue was dissolved in deionized water. The pentavalent oxidation state of NpO_2^+ was obtained by potentiostatic electrolysis and its purity was verified by UV Vis/NIR spectroscopy (Sjoblom and Hindman, 1951). The final Np concentration was determined by LSC.

2.2. Illite preparation and characterization

Purified Na illite was used in this work and was provided within the EC project CP CatClay (www.catclay.org). The source material is derived from lacustrine continental sediments deposited at the Upper Eocene (~ 35 Ma) in the basin of Le Puy en Velay (Massif Central, France). The clay formation in this region is mainly composed of illite with small contributions of kaolinite, a 1:1 clay mineral. In addition to kaolinite, K feldspar, quartz and calcite are present in varying amounts (between 0% and 40%; Gabis, 1963). The <63 μm size fraction was obtained by grinding and sieving the raw material (Poinssot et al., 1999). The purification procedure aims at removing non clay (Ca rich) mineral phases and converting the illite to the Na form. The received illite material was equilibrated in a formate buffer solution (0.05 M formic acid and 0.05 M Na formate in 1 M NaCl, pH ~ 3.5) at a mass to volume ratio (m/V) of 100 g/L for 4 h by gentle magnetic stirring. The solid phase was separated by centrifugation (500 g for 5 min), re suspended in 1 M NaCl and equilibrated overnight (gentle magnetic stirring). This washing procedure was applied three times. After removing 80 85% of the liquid phase, the settled suspension was transferred into dialysis tubes and dialyzed against MilliQ water. The external solution was replaced twice daily, until no NaCl was detectable in the external solution (checked by adding $AgNO_3$). In the last step, the clay suspensions were freeze dried. The characterization of the illite material is given in the supporting information file. The illite contains 7 wt.% Fe_2O_3.

2.3. Determination of pH and Eh

The pH in the clay suspensions was measured by an Orion 525A pH meter with a Ross electrode calibrated with 4 standard buffers (pH 3, 5, 7 and 9; Merck). The error of pH measurements is ±0.05. The redox potentials in the clay suspensions were measured using an Orion 525A (Eh meter) and a Pt combined electrode with Ag/AgCl reference system (Metrohm) and converted into Eh versus standard hydrogen electrode (SHE) by correcting for the potential of the reference electrode. A commercial redox buffer (220 mV, Schott instruments) was used for calibration. An equilibration time of 15 min was applied for all Eh measurements. The suspension was stirred prior to the Eh measurement. Uncertainties in Eh measurements lie in a range of ±50 mV (Altmaier et al., 2010; Kirsch et al., 2011). Eh was converted to the apparent electron activity, $pe = \ \log a_{e-} = 16.9 \times Eh(V)$ at 25 °C, and the error of pe data is equal to around ±0.8.

2.4. Batch sorption experiments

All sorption experiments were performed as batch type experiments at initial Np(V) concentrations in the range of $3 \times 10^{-8}\ \ 3 \times 10^{-4}$ M. Maximum Np concentration is below the solubility limit of relevant Np(V) bearing solids (Guillaumont et al., 2003). The batch experiments were carried out in 40 mL polypropylene centrifuge tubes at room temperature in an argon glove box (<1 ppm O_2, absence of CO_2). The sample volume was 25 mL. At a solid to liquid ratio of 2 g/L, the suspensions were preconditioned in 0.1 M NaCl by shaking continuously for 4 5 days to achieve a given target pH value by adding 0.1 M HCl or 0.1 M NaOH. After mixing the NpO_2^+ solution with the preconditioned illite suspension, pH was readjusted by adding acid or base (HCl/NaOH). The samples were shaken end over end and Np sorption was followed with time after the addition of NpO_2^+ to the illite suspension. After 7, 21, 35 and 63 days, pH and Eh were measured in the suspension and an aliquot of each sample was centrifuged in a Beckman L7 Ultracentrifuge at 90,000 rpm for 1 h. The supernatant was analyzed for dissolved Np by LSC. Results obtained in batch experiments will be expressed throughout as distribution coefficients (R_d in L/kg), calculated by the following equation:

$$R_d = \left([Np]_{tot}/[Np]_{aq} \quad 1\right) \times V/m \qquad (1)$$

where $[Np]_{aq}$ and $[Np]_{tot}$ (mol/L) are the dissolved (final) equilibrium and total (initial) concentrations of Np in solution, respectively. The term V/m corresponds to the aqueous solution volume to illite mass ratio (L/kg). An uncertainty of ±0.3 is commonly associated with $\log R_d$ determination for radionuclide sorption to clay minerals (Bradbury and Baeyens, 2009a), although for low $[Np]_{tot}$ and high uptake, the uncertainty on $\log R_d$ might be higher.

A test experiment was performed to determine the oxidation state of Np(i) for a solution in contact with illite and (ii) for the illite surface via two liquid liquid extraction methods using either 1 phenyl 3 methyl 4 benzoylpyrazolone 5 (PMBP)or phosphoric acid bis (2 ethyl hexyl) ester) (HDEHP) (Bertrand and Choppin, 1982; Nitsche et al., 1988, 1994) as extracting agents. For our experimental conditions, both methods are equivalent: PMBP extracts Np(IV) whereas HDEHP extracts Np(V) in organic phase at pH = 0. Results obtained with both methods were in good agreement. The experiment was carried out under Ar atmosphere. One sample (pH = 7.0; $[Np]_{tot} = 10^{-5}$ M; [NaCl] = 0.1 M; m/V = 2 g/L) was filtered using 10 kDa filters (5000 rpm for 1 h) after one week contact time to separate solid from solution. To 0.6 mL portion of the filtrate solution 0.2 mL 2 M HCl and either 0.8 mL 0.025 M PMBP in Xylene or 0.5 M HDEHP in Toluene was added and then vigorously shaken for 10 min. The aqueous and organic phases were separated by centrifugation for 30 min (5000 rpm) and aliquots of each phase were taken for radiometric analysis. The solid (i.e. illite) was re suspended in 1 M HCl for 2 days. Then the phases were separated by ultrafiltration (10 kDa). The mass of solid that was recovered from the filter was not determined so the faction of Np desorbed in 1 M HCl cannot be determined. Only the redox speciation of Np in the desorbed fraction is obtained and discussed.

2.5. X-ray absorption near-edge spectroscopy (XANES)

Two samples were prepared as described in the previous section for Np L_3 XANES measurements. Initial conditions were $[NpO_2^+]_{tot} = 3 \times 10^{-4}$ M, m/V = 20 g/L. Although XANES analysis requires higher Np concentration than those studied in the sorption experiments, the spectroscopic study yields direct evidence as to whether Np redox speciation is affected in the presence of illite. The final pH values were 7.4 and 9.6, respectively, for the two samples, and Eh was 0.40 ± 0.05 V (pe = 6.8 ± 0.8) for both samples. An aliquot of each sample was centrifuged at 3000 g in a polyethylene vial (500 μL). The supernatant was discarded and an aliquot was taken for LSC. The wet illite paste was transferred into a vial, mounted inside an Ar flushed cell which acts as second containment, keeping sample vials in an anaerobic atmosphere (Brendebach et al., 2009). Measurements were performed at the 2.5 GeV synchrotron light source ANKA, KIT, Germany, at the INE Beamline for actinide research (Rothe et al., 2006, 2012). A pair of Ge(422) crystals was used in the Lemonnier type double crystal monochromator (DCM). The monochromatic radiation is focused by a Rh coated to roidal mirror into a spot of <1 mm × 1 mm at the sample position. Higher harmonic radiation in the incident beam was suppressed by detuning the parallel alignment of the DCM crystals to 70% of photon flux peak intensity in the middle of the spectral range at the beginning of each scan. The incident flux was measured by an Ar filled ionization chamber at ambient pressure and held constant by a digital MOSTAB feedback system. The Np L_3 edge spectra ($E(Np^0\ 2p_{3/2}) = 17.61$ keV) were calibrated against the first derivative XANES spectrum of a Zr foil (energy of the first inflection point set to $E(Zr^0\ 1s) = 17.998$ keV). All Np L_3 XANES spectra were recorded in fluorescence detection mode by registering the Np L_α fluorescence yield at ~13.95 keV as a function of the incident photon energy with a 5 pixel Ge solid state detector (Canberra LEGe). Up to 5 scans were collected at room temperature and averaged for each sample. The illuminated area of the sample was changed between each scan to minimize potential Np redox reactions induced by the beam. XANES spectra were isolated from XAFS scans following subtraction of a linear pre edge background function and normalization of the edge jump to unity using the Demeter Athena software (Ravel and Newville, 2005).

2.6. Thermodynamic modeling

pe pH diagrams for Np were obtained using PhreePlot (Kinniburgh and Cooper, 2009), which contains an embedded version of the geochemical speciation program PHREEQC (Parkhurst and Appelo, 1999). PhreePlot also includes a parameter optimization procedure, which automatically fits a model to experimental data by minimizing the weighted sum of squares of the residuals. A modified Marquardt Levenberg procedure (Powell, 1965) was applied. With this method, PhreePlot provides also a statistical uncertainty of the estimated parameters. Thermodynamic constants for Np aqueous speciation were taken from the NEA thermodynamic database (Guillaumont et al., 2003). The 2 site protolysis non electrostatic surface complexation and cation exchange model (2 SPNE SC/CE model) was used to simulate Np sorption to illite (Bradbury and Baeyens, 2009b). The cation exchange capacity (CEC) of the illite was set equal to 0.225 eq/kg. Two types of proton active sites are necessary to describe the titration data, but only one type is assumed by the model approach to bind cations. Among these cation binding sites, weak sites ([WOH] = 4×10^{-2} mol/kg) as well as less abundant strong sites ([SOH] = 2×10^{-3} mol/kg) are defined in this model with the same acid base properties. Bradbury and Baeyens (2009b) determined a NpO_2^+ Na^+ selectivity coefficient as well as Np(V) surface complexation constants for illite within the 2 SPNE SC/CE model. Due to the weak Np(V) sorption to illite, leading to low surface coverage, only Np(V) surface complexation constants for the strong sites were determined. Bradbury and Baeyens (2009b) derived a linear free energy relationship (LFER) for the strong sites in the 2SPNE SC/CE model, which can be used to estimate surface complexation constants for cations, where experimental data are not available. LFER relates the hydrolysis constants of metal ions ($^{OH}K_x$, where x represents the number of OH^- in the complex, Eq. (2)) to their surface complexation constants ($^{S}K_{x-1}$, Eq. (3)):

$$M^{n+} + x\,H_2O = M(OH)_x^{(n-x)} + x\,H^+;\, ^{OH}K_x \tag{2}$$

$$\begin{aligned} &SOH + M^{n+} + (x\quad 1)H_2O \\ &= \quad SOM(OH)_{(x-1)}^{(n-x)} + x\,H^+;\, ^{S}K_{(x-1)} \end{aligned} \tag{3}$$

$$\log{}^{S}K_{(x-1)} = 7.9 \pm 0.4 + (0.83 \pm 0.02) \times \log{}^{OH}K_x \tag{4}$$

Eq. (4) represents the LFER where M^{n+} is a metal ion with a charge of $+n$. In the present study, the LFER is used to estimate surface complexation constants for Np(IV). These constants will be used as a starting point when fitted to the present experimental data using PhreePlot. A weight of 1 will be applied to all data. The error between experimental and modelled R_d values (with the fitted constant showing the best fit) is recalculated as the root mean squared deviation (RMSD). A summary of all parameters for the 2SPNE SC/CE model used in the present study is given in Table 1. Additional information provided in Table 1 will be discussed below.

Table 1
Reactions and respective thermodynamic constants used in the present modeling section.

Reaction	log K (I = 0)
$NpO_2^+ + 4H^+ + e \ \ = Np^{4+} + 2H_2O$	10.21
$NpO_2^+ + H_2O = \equiv NpO_2OH + H^+$	11.3
$NpO_2^+ + 2H_2O = \equiv NpO_2(OH)_2 \ + 2H^+$	23.6
$Np^{4+} + H_2O = NpOH^{3+} + H^+$	0.55
$Np^{4+} + 2H_2O = Np(OH)_2^{2+} + 2H^+$	0.35
$Np^{4+} + 3H_2O = Np(OH)_3^+ + 3H^+$	2.3 (Pu)
$Np^{4+} + 4H_2O = Np(OH)_4 + 4\ H^+$	8.3
$NpO_{2(am)} + 2\ H_2O = Np^{4+} + 4\ OH$	56.7
$X\ Na + NpO_2^+ = X\ NpO_2$	0^f
$\equiv SOH + H^+ = \equiv SOH_2^+$	4^f
$\equiv SOH = \equiv SO \ \ + H^+$	6.2^f
$\equiv SOH + NpO_2^+ = \equiv SO{-}NpO_2 + H^+$	2.0^f
$\equiv SOH + NpO_2^+ + H_2O = \equiv SO{-}NpO_2OH \ \ + 2H^+$	10.3^f
$\equiv SOH + Np^{4+} = \equiv SO{-}Np^{3+} + H^+$	nd (8.4 ± 0.6)
$\equiv SOH + Np^{4+} + H_2O = \equiv SO{-}NpOH^{2+} + 2H^+$	nd (8.2 ± 0.7)
$\equiv SOH + Np^{4+} + 2H_2O = \equiv SO{-}Np(OH)_2^+ + 3H^+$	6.4 ± 1.2 (6.0 ± 0.7)
$\equiv SOH + Np^{4+} + 3H_2O = \equiv SO{-}Np(OH)_3 + 4H^+$	0.7 ± 1.3 (1.0 ± 1.1)
$\equiv SOH + Np^{4+} + 4H_2O = \equiv SO{-}Np(OH)_4 \ + 5H^+$	5.7 ± 1.2 (nd)

Aqueous reaction constants and the solubility product of $NpO_{2(am)}$ are taken from Guillaumont et al. (2003). The missing $Np(OH)_3^+$ formation constant is taken from the analogue $Pu(OH)_3^+$."f" denotes fixed parameters during the fitting procedure, taken for Bradbury and Baeyens (2009a,b). Np(IV) surface complexation constants are fitted from the present experimental results associated with their uncertainty. Calculated values using a LFER are shown for comparison between parentheses. "nd" refers to values that could not be determined.

3. RESULTS AND DISCUSSION

3.1. Experimental Np-illite sorption data

Fig. 1 presents Np sorption to illite (R_d in L/kg) as a function of pH (i.e. pH edge). Only the highest and the lowest Np total concentrations investigated in the present study at various pH are presented here: $[Np]_{tot} = 10^{-6}$ M (Fig. 1a) and 3×10^{-8} M (Fig. 1b). Results obtained for intermediate $[Np]_{tot}$ are consistent with those data. The complete dataset is provided within the supplementary file. R_d values determined after different reaction times (7, 21, 35 and 63 days) are presented. For comparable pH, no clear evolution of R_d values with time for the two total Np concentrations presented here is observed after 7 days. For $[Np]_{tot} = 10^{-6}$ M (Fig. 1a), most of the data being recorded for pH <8 show only a small increase of R_d with pH, which is consistent with the weak surface complexation of Np(V) at the edges of clay particles. For $[Np]_{tot} = 3 \times 10^{-8}$ M (Fig. 1b) and pH <6, R_d values are relatively similar to those measured at higher metal ion concentration. However, a significant increase of R_d is observed for pH >6 with values being 1 2 orders of magnitude higher than for experiments with $[Np]_{tot} = 10^{-6}$ M. Slightly more scattering R_d values are observed for $[Np]_{tot} = 3 \times 10^{-8}$ M but the sorption results are reproducible within an experimental uncertainty for $\log R_d$ of about ±0.5. When increasing $[Np]_{tot}$, pH edges are shifted to higher pH, i.e. a decrease of R_d with increasing $[Np]_{tot}$ is observed at a given pH. This is consistent with non ideal sorption behavior of Np. Sorption data for $pH = 7.2 \pm 0.2$ are plotted as $\log R_d$ versus $\log\ [Np]_{tot}$ in Fig. 1c, which further illustrates the non ideal sorption behavior.

3.2. Comparison with the sorption behavior of other metal ions

Sorption isotherms for various metal ions recorded at $pH = 7.2 \pm 0.2$ are plotted in Fig. 2. In the logarithmic plot, our Np sorption data follow a linear relationship with a slope of approximately 0.4, which indicates non ideal sorption behavior (Freundlich, 1909). This means that either various surface sites are present or more than one sorption mechanism occurs. Our experimental results are compared with Sr(II) , Ni(II) and Eu(III) illite sorption isotherms for pH = 7, in 0.1 M $NaNO_3$, NaCl or $NaClO_4$) (Poinssot et al., 1999; Bradbury and Baeyens, 2005) taken from the literature. We included a data set for U(VI) sorption onto montmorillonite (Marques Fernandes et al., 2012) at pH = 6.8 as data for illite at pH ≈ 7 are not available. The two clay minerals have similar sorption properties at pH = 7. Although the cations shown in Fig. 2 have very different chemical behavior, they all exhibit linear sorption isotherms (slope ~ 1) up to a surface coverage of approximately 10^{-3} mol/kg where the so called "strong sites" dominate cation surface speciation (e.g. Bradbury and Baeyens, 2009a,b). The observed non ideal Np illite sorption isotherm down to 10^{-5} mol/kg is therefore inconsistent with data reported for other cations and opposes the assumption of a pronounced site heterogeneity and rather suggests the existence of different sorption mechanisms.

Fig. 3 compares sorption data obtained within the present study ($[Np]_{tot} = 1.2 \times 10^{-7}$ M, m/V = 2 g/L; data are not shown in Fig. 1) with those reported by Gorgeon (1994) for illite obtained under aerobic conditions and $[NaClO_4] = 0.1$ M ($[Np]_{tot} = 10^{-6}$ M, m/V = 10 g/L). Additionally, a comparison with reported Np sorption data

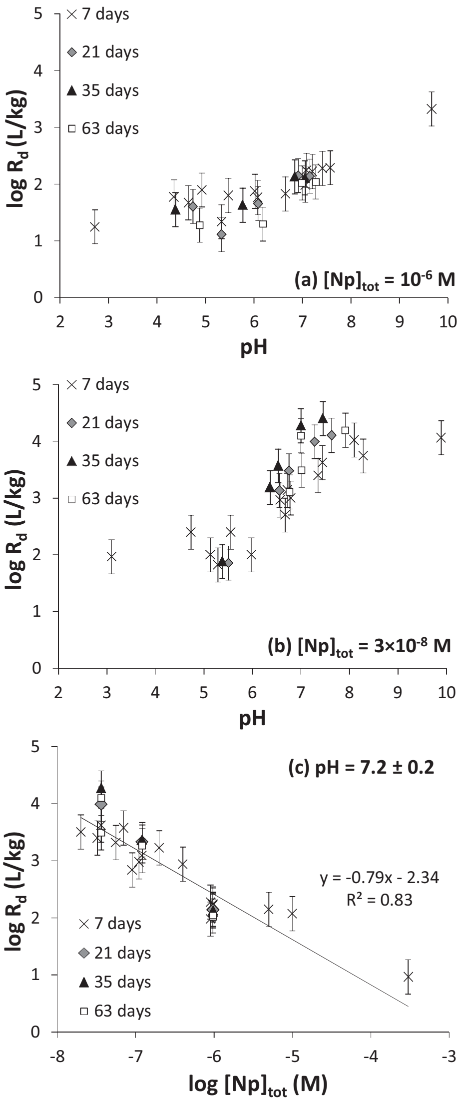

Fig. 1. Np sorption to illite (R_d, in L/kg) versus pH measured for different reaction time (7, 21, 35, 63 days) and a Np total concentration of (a) 10 ^{6} M and (b) 3 × 10 ^{8} M. (c) Results obtained for pH = 7.2 ± 0.2 are plotted as log R_d versus $[Np]_{tot}$.

on montmorillonite is provided in Fig. S3 (data form Gorgeon, 1994; Turner et al., 1998; Bradbury and Baeyens, 2006), which corroborate the following interpretation. Gorgeon's R_d values lie clearly below the data obtained in our study. A possible reason for the difference might be, that the influence of atmospheric CO_2 and concomitant Np carbonate complexation cannot be excluded completely in the experiments of Gorgeon (1994), even though contact with atmospheric CO_2 was limited by capping the sample after pH adjustment. Turner et al. (1998) observed that atmospheric CO_2 decreased Np(V) sorption to montmorillonite only at pH > 8 (Fig. S3). Therefore, the impact of CO_2 on Gorgeon's data for Np(V) sorption onto illite should be of minor importance. Sorption to accessory minerals left over from incomplete purification appears very unlikely in our experiments. Such mineral

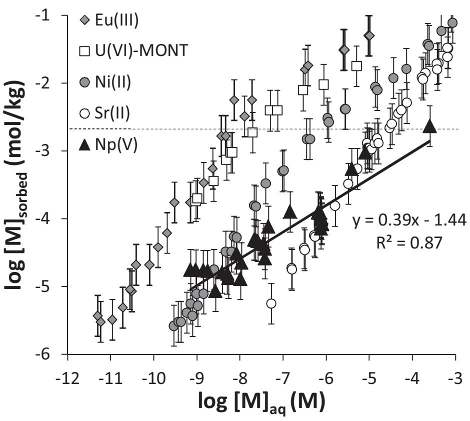

Fig. 2. The present Np illite sorption isotherm for pH = 7.2 ± 0.2, fitted with a Freundlich equation, is compared with literature data for other cations (noted "M") sorption to illite (Eu(III), Ni(II), Sr(II); Poinssot et al., 1999; Bradbury and Baeyens, 2009a,b) and U(VI) sorption to montmorillonite (noted "U(VI) MONT"; Marques Fernandes et al., 2012). Dotted line shows the illite and montmorillonite strong binding sites surface density (2 × 10 ^{3}mol/kg) considered in the 2 SPNE SC/CE model.

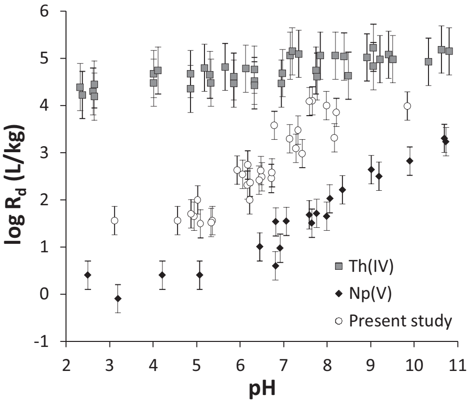

Fig. 3. Np sorption to illite (R_d, in L/kg) versus pH measured for a Np total concentration of 1.2 × 10 ^{7} M and compared with literature Np(V) and Th(IV) illite sorption data (Gorgeon, 1994; Bradbury and Baeyens, 2009b). The present experimental conditions are comparable to the one of Gorgeon (1994), except that the results were obtained in ambient atmosphere in the latter study.

phases could not be identified by XRD. Also, by comparison with literature data for Np(V) sorption onto montmorillonite (Fig. S3), which shows a higher CEC than illite, some of our R_d data are by one order of magnitude higher for pH <6. According to Bradbury and Baeyens (2009b) Np(V) sorption onto illite is controlled by cation exchange at pH <6. They simulated the results of Gorgeon (1994) using a selectivity coefficient for the exchange of Na^+ by NpO_2^+ equal to 1. Such a coefficient appears to be reasonable for the 1:1 exchange of cations with a formal charge of +1. A similar treatment with our data would lead to NpO_2^+ Na^+ exchange constants in a range of 30 100.

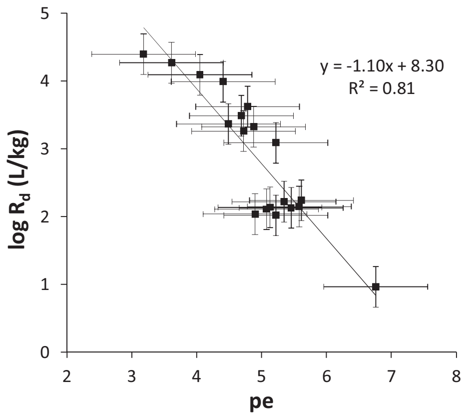

Fig. 4. Log R_d versus the apparent electron activity pe (= log a_e = 16.9 Eh(V)) for pH = 7.2 ± 0.2.

Neither the presence of CO_2 nor minor impurities can explain such observation. The major difference between Gorgeon's and our experiments is the different atmospheres: Gorgeon kept the samples under air (oxidizing conditions) while the present results were obtained in an Ar glovebox. A comparison with sorption data obtained for Th(IV) (Bradbury and Baeyens, 2009b) (Fig. 3) shows that our R_d values appear to fall in between those for Np(V) and Th(IV). This may hold as a first indication for the partial reduction of Np(V) to Np(IV) under our experimental conditions. Another hint in this direction is given in Fig. 4 which contains log R_d plotted versus pe for Np sorption at pH = 7.2 ± 0.2. Despite the relatively large experimental uncertainty for pe, there is a clear correlation of log R_d increasing with decreasing pe. Lowest pe values are measured for those samples with lowest total Np concentrations. In other words, Np(V) reduction becomes predominant at low total metal concentrations and thus is responsible for the non ideal sorption isotherm (Fig. 1c or 2). Furthermore, the total Np concentration seems to influence the measured pe value. Interestingly, the slope of log R_d versus pe approximates unity, which is consistent with the reduction of Np(V) to Np(IV)by a one electron transfer mechanism.

Finally, a redox state analysis applied to one of the samples (pH = 7.0; $[Np]_{tot} = 10^{-5}$ M; [NaCl] = 0.1 M; m/V = 2 g/L) also corroborates the partial reduction of Np(V) to Np(IV) on the illite surface. After one week contact time, only Np(V) is found in solution (93 ± 10%). After re suspending the illite in 1 M HCl for 2 days, a significant amount of the desorbed Np is found to be Np(IV) (41 ± 10%). As stated before, the amount of Np that may have remained on the illite after the acid treatment was not determined. However, Np(V) sorbs weakly to minerals and should be more easily desorbed than the strongly adsorbing Np(IV) (Powell et al., 2004, 2005). If Np remained sorbed after the acid treatment, it would be very likely Np(IV). Therefore, this experiment is not able to provide quantitative information on surface Np redox speciation, because it might underestimate the amount of Np(IV). It is, however, sufficient to demonstrate that a significant amount of Np(IV) is present at the illite surface.

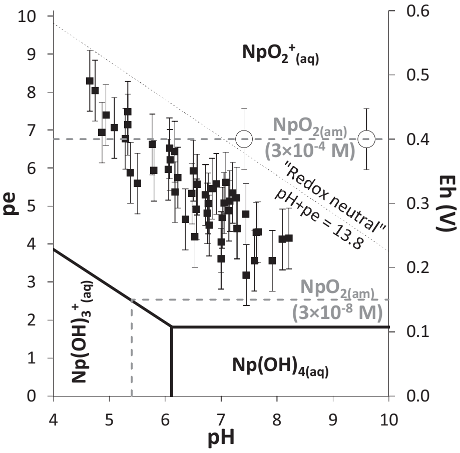

Fig. 5. pH Pe (or Eh on the secondary scale) diagram of Neptunium in 0.1 M NaCl solution. Experimental results are presented as black squares for the batch experiments and large white circles for the two samples analyzed by XANES. The formation of $NpO_{2(am)}$ is also included in the calculations for the lowest and the highest $[Np]_{tot}$ investigated (3×10^{8} and 3×10^{4} M) and its predominance field is delimited by grey dotted lines.

3.3. Redox conditions

The pH pe(Eh) diagram for Np in 0.1 M NaCl is shown in Fig. 5. The measured pH pe values are presented for the batch experiments performed at relatively low $[Np]_{tot}$ (black squares) and two samples at relatively high $[Np]_{tot}$ (3×10^{-4} M, large white circles) prepared for analysis with spectroscopic techniques. Redox borderlines for all experiments are included, as well, by considering the possible precipitation of Np(IV) (hydr)oxide ($NpO_{2(am)}$) at total Np concentrations of 3×10^{-8} M and 3×10^{-4} M, respectively. "Redox neutral" conditions are also shown for comparison (pH + pe = 13.8; see e.g. Neck et al. (2007) for more details). For low Np concentrations all experiments are clearly located in the predominance field of Np(V), as also observed by the redox state analysis of Np in the supernatant. Those data at a first glance cannot justify the hypothesis of Np(V) reduction in presence of Na illite. At high Np concentrations, however, pe data hit the redox borderline, suggesting the establishment of an equilibrium with solid $Np(IV)O_{2(am)}$ and Np(V) species in solution. Note that surface sorption equilibria are not taken into account for those scoping calculations.

3.4. Spectroscopic results

Np redox speciation at the illite surface is further investigated by XANES. The Np L_3 XANES measured at pH = 7.4, m/V = 20 g/L and 3×10^{-4} M of Np (initially introduced as NpO_2^+) is presented on Fig. 6a. This sample contains the highest $[Np]_{tot}$ and exhibits as well the highest pe (pe = 6.8 ± 0.8). Under those conditions 15% of the total Np is sorbed onto illite (i.e. 2.3×10^{-3} mol/kg). As explained before, phase separation was performed to remove the solution from the sample. Therefore, the

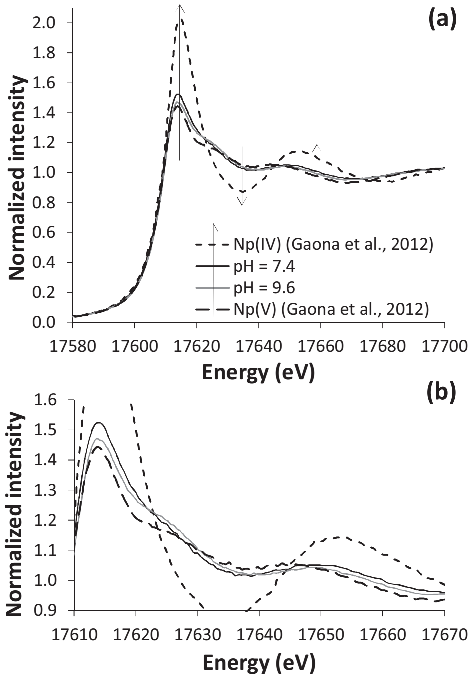

Fig. 6. (a) Np L3 XANES measured for a Np illite sample prepared at $pH = 7.4$ and $9.6([Np]_{tot} = 3 \times 10\ ^{4}$ M, $m/V = 20$ g/L, $Eh = 0.40 \pm 0.05$ V). Reference XANES of aqueous Np(IV) and Np(V) in 1 M $HClO_4$ from Gaona et al. (2012) are shown for comparison. Arrows highlight a Np(V) reduction to Np(IV) process in the present study. The area between 17,610 and 17,670 eV is enlarged in (b).

following analysis will refer only to the amount on Np present in the solid phase (i.e. 15% of the initially introduced Np). The presence of a shoulder at 17,625 eV, indicating multiple scattering of the outgoing Np $2p_{3/2}$ electron along the axis of the NpO_2^+dioxo cation, shows the dominance of the +V redox state. However, the "white line" (WL) position as well as the inflection point of Np redox states +IV and +V is relatively similar and cannot be used as a conclusive probe for Np redox speciation. Nevertheless, Np(V) and Np(IV) XANES show significant differences in the intensity of the WL. Previously published XANES, measured at the same beam line, were selected for this purpose. XANES spectra of the NpO_2^+ and Np^{4+}aquo ions in 0.1 M $HClO_4$ from Gaona et al. (2012) are used as references for Np(V) and Np(IV). When plotted together, the Np illite XANES for $pH = 7.4$ shows significant differences compared to a Np(V) reference, especially an increase in WL intensity (Fig. 6). The same energy range is considered for the pre edge and for the normalization of all XANES spectra (pre edge: 17.30 17.55 keV; post edge: 17.77 18.20 keV) and careful preliminary tests were made to ensure that the observed differences in the XANES are not due to the normalization procedure. Additionally, a decrease at ~17,635 and an increase at ~17,660 eV are observed. These two observations are consistent with the presence of a mixture of Np(V) and Np(IV).

As pointed out by Denecke et al. (2005), the determination of Np redox speciation by XANES analysis can be difficult under certain conditions. In their study, a sample containing Np(IV) was partially oxidized to Np(V), leading to a decrease in WL intensity. Because the white line height decreases substantially going from ions in solution to solids (condensed system), it could have been erroneously attributed to the formation of Np(IV) (hydr)oxides, if the composition of the sample had been unknown. In the present study, the situation is different. The WL of Np(V) sorbed to a mineral surface cannot be more intense than that of Np(V) aquo ion. Therefore, the present results can confidently be attributed to the presence of Np(IV). By fitting the Np illite XANES with a linear combination of Np(V) and Np(IV) reference samples, 14% of the adsorbed Np is determined to be Np(IV). The result of the linear combination fit(LCF) is shown in Fig. S4. Although this value is small, it must be considered as a minimum value since the aquo ions exhibit the most intense WLs. The same exercise with either a Np(V) or a Np(IV) reference, where Np is in a more condensed state (i.e. with a less intense WL), would lead to a larger fraction of Np(IV). No further attempt was made to accurately determine the amount of Np(IV), and the spectroscopic result is taken to corroborate the redox state analysis by liquid liquid extraction showing that Np(V) reduction to Np(IV) can occur in the presence of illite.

An additional sample is analyzed by XANES under similar initial conditions but at $pH = 9.6$. The measured pe does not significantly differ from that obtained at $pH = 7.4$ ($pe = 6.8 \pm 0.8$). Invariant pe at higher pH implies more oxidizing conditions in this additional sample. Due to the higher pH, 90% of Np is sorbed to the illite surface (1.3×10^{-2} mol/kg), which can be partly attributed to the stronger surface complexation of Np(V) to illite (Gorgeon, 1994) at this pH. The Np L_3 XANES of the sample for $pH = 9.6$ is also shown in Fig. 6. It shows a less intense WL compared to $pH = 7.4$. The LCF using the XANES spectra of NpO_2^+ and Np^{4+}aquo ion shows that only 5% of the adsorbed Np at the illite surface is Np(IV) (Fig. S4). Given the uncertainty of the measured pe, the stability of a fraction of Np(IV) in the present samples is also qualitatively in agreement with thermodynamic calculations, considering the formation of $NpO_{2(am)}$ (Fig. 5).

3.5. Surface complexation modeling

The aim of the present section is to attempt a complete description of Np sorption and concomitant redox reactions in presence of illite as a function of pH, pe and $[Np]_{tot}$. Assuming that the Np illite system in each sample is in equilibrium, the data might be simulated by taking into account constants for the respective redox, complexation and surface sorption reactions.

Surface complexation calculations are made with the 2 SPNE SC/CE model. We only consider strong sites at the illite surface and thus constrain the modeling exercise to experimental data obtained at total Np concentrations up to 10^{-6} M. Only the sorption data with experimentally determined pe are considered because pe is necessary to calculate Np redox speciation according to the first equation in Table 1. We furthermore take surface complexation constants and selectivity coefficients (Bradbury and Baeyens, 2009b) derived from Gorgeon's data obtained under aerobic conditions to describe sorption of Np(V) species. Cation exchange reactions are not considered for Np(IV) species as they are assumed irrelevant for tetravalent metal ions (Bradbury and Baeyens, 2009b). Np(IV) illite surface complexation constants values estimated from the LFER (Eq. (4)) are taken as starting points and fitted to the experimental log R_d data using PhreePlot. According to the 2 SPNE SC/CE model for the sorption of Th(IV) (Bradbury and Baeyens, 2009b), SO $Np(OH)_4^-$ is expected to be the dominant Np(IV) surface species at least for $pH > 7$. An approximation for the respective surface complexation constant by LFER was not possible because it requires a complexation constant for $Np(OH)_5^-$, for which no value has been selected in the NEA database (Guillaumont et al., 2003). We, therefore, took literature data for the SO $Th(OH)_4^-$ complex as an initial value for the fitting. Note that additional sensitivity tests showed that the fitting procedure converged to very similar constants independent of the initial values. As a result, we obtained values for surface complexation constants for Np(IV) as given in Table 1. Values estimated by applying the LFER are given in brackets and are very similar to the fit results. The uncertainties for respective log K values are composed of contributions arising from (i) the statistical uncertainty associated with the fitting procedure, calculated by PhreePlot (between 0.1 and 0.2 log units), (ii) the experimental error in pe (i.e. ±0.8) and (iii) the experimental error in log R_d (i.e. ±0.3). The results are presented in Fig. 7 for the complete dataset used to fit the surface complexation constants for Np(IV). Fig. 7a c shows log R_d versus pH for the three series of experiments with $[Np]_{tot} = 10^{-6}$, 10^{-7} and 3×10^{-8} M, respectively. Experimental log R_d and the corresponding calculated values with the fitted constants are shown, respectively, as black and white symbols. Fig. 7c e shows the corresponding redox conditions for each series on a pH pe(Eh) diagram. In

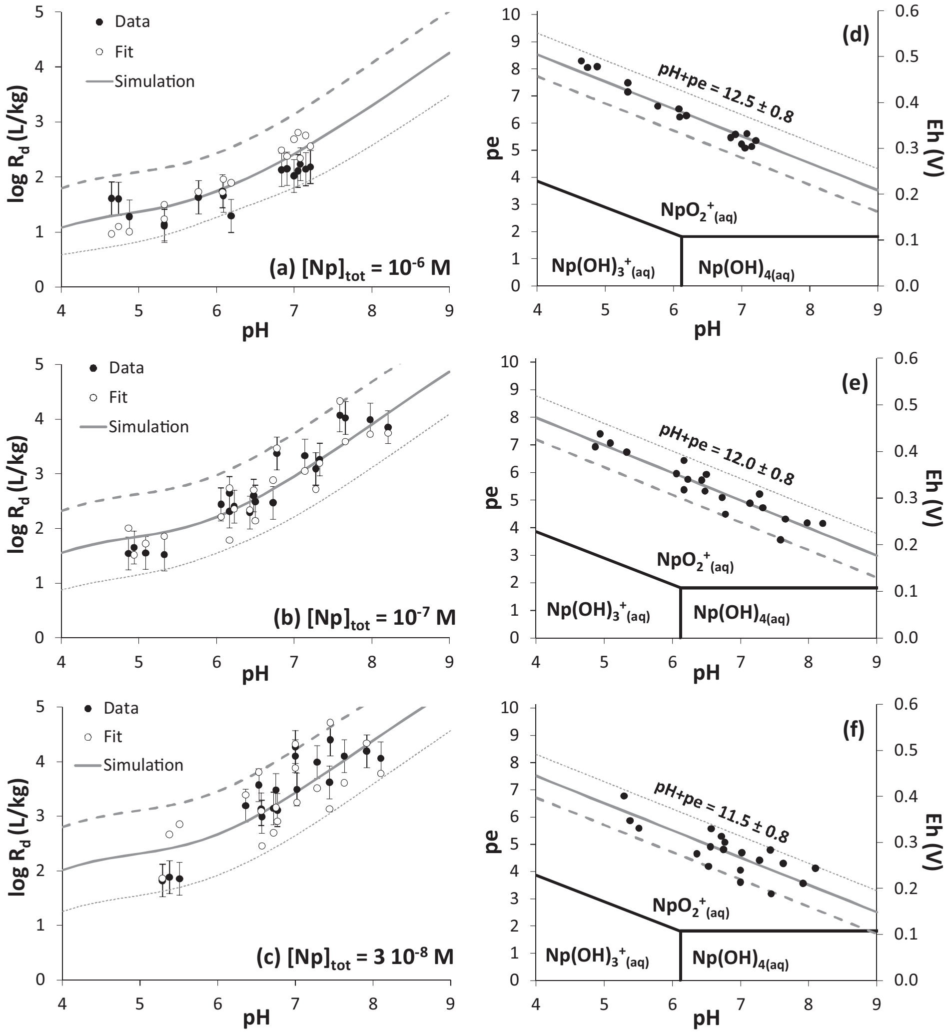

Fig. 7. Experimental log R_d (black circles) and the corresponding calculated values (white circles) with the fitted surface complexation constants for Np(IV) with illite versus pH for $[Np]_{tot} = 10^{\ 6}$ (a), $10^{\ 7}$ (b) and $3 \times 10^{\ 8}$ M (c). The corresponding redox (pH pe/Eh plot) conditions are shown on the right side with the predominance diagram for aqueous Np species (d) (e) (f). Lines represent calculations made for constant pH + pe (bold line) ± 0.8 (lower limit: bold dashed line; upper limit: thin dashed line).

addition, calculations with constant redox conditions (i.e. constant pH + pe values) for each series in the range of the expected experimental uncertainty (i.e. ±0.8 pe units/ ±50 mV) illustrate the coupled effect of pH and pe on Np sorption to illite. The increase of log R_d with decreasing $[Np]_{tot}$ is well described. Actually, this behavior is directly related to the redox conditions: on average pH + pe decreases from 12.5 to 11.5 with $[Np]_{tot}$ decreasing from 10^{-6} to 3×10^{-8} M. Calculated sorption of Np to illite is very sensitive to the pe. This can be seen (i) in the simulations, where ±0.8 pe units leads to important variations in log R_d for a given pH value and (ii) in the results of the fit, where scattering in the experimentally determined pe also leads to scattering in the log R_d values. The latter observation might explain why our Np sorption results seem to exhibit larger uncertainty than commonly assumed (i.e. ±0.3 log R_d units). Additionally, the results of the fit are shown for $pH = 7.2 \pm 0.2$ and as a plot of calculated versus experimental log R_d for the complete dataset (i.e. for the various pH, pe, contact time, and $[Np]_{tot}$) in Fig. S5. Average differences between calculated and experimental log R_d data (based on the RMSD) is found equal to 0.36, which lies in the same range as experimental uncertainties. Speciation calculations furthermore give no evidence for the precipitation of $NpO_{2(am)}$ under any investigated condition. Due to the predominance of Np(V) in solution and the strong surface complexation of Np(IV) to illite, aqueous Np(IV) concentrations remain below solubility limits with regard to $NpO_{2(am)}$.

In order to check the reliability of the fitted log K value for the SO Np(OH)$_4^-$ surface complex, we performed predictive simulations of Np(IV) sorption to illite (log R_d versus pH) using the constant in Table 1. Those calculated data are then compared with experimental data for Sn(IV) and Th(IV) taken from the literature (Bradbury and Baeyens, 2009a,b) (Fig. 8). Experimental R_d values for both tetravalent metal ions are very similar and invariant in the pH range from 3 to 11. Taking the relatively large confidence interval into account simulated log R_d values for Np(IV) and Sn(IV), Th(IV) are quite consistent. Note that the surface complexation constants for Np(IV) (Table 1) are larger than previously reported for Th(IV) (Bradbury and Baeyens, 2009b). This observation is consistent with the stronger hydrolysis of Np(IV) than Th(IV) according to the LFER of Bradbury and Baeyens (2009b).

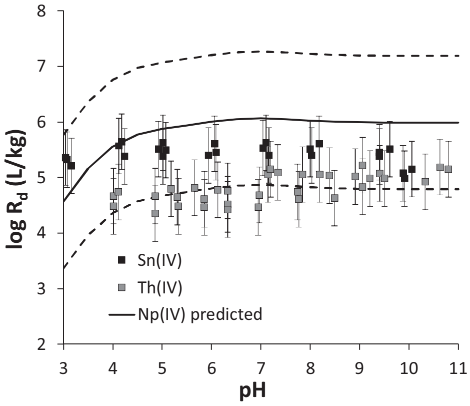

Fig. 8. The predicted Np(IV) illite pH edge (log R_d versus pH) with the presently determined constants is compared with the experimental pH edge of Th(IV) and Sn(IV). Dotted lines represent the uncertainty on the determined surface complexation constants for Np(IV) illite.

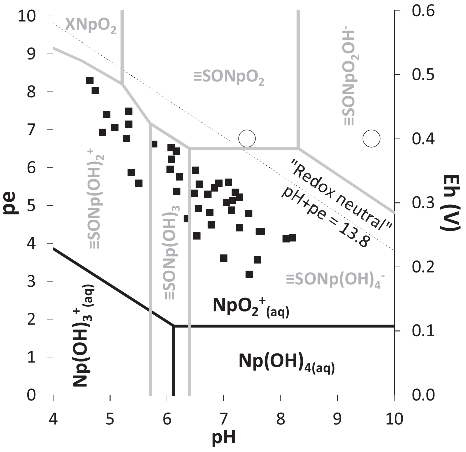

Fig. 9. On the pH pe (or Eh on the secondary scale) diagram of Neptunium in 0.1 M NaCl solution presented in Fig. 5, is superimposed Np predominance diagram calculated at the illite surface. It shows that the Np(V)/Np(IV) borderline at the illite surface is between 3 and 5 pe units (0.18 0.30 V), depending on the pH, higher than the corresponding one in solution. Experimental pH pe values are also plotted (without error bars for clarity), showing that in the present batch experiments, Np(V) prevails in solution whereas and Np(IV) prevails at the surface, explaining the stronger Np illite sorption observed compared with literature, under aerobic condition.

3.6. Np(V)/Np(IV) redox speciation in presence of illite

Based on constants given in Table 1, PhreePlot was used to construct a predominance diagram for Np surface speciation for the range $4 < pH < 10$ (Fig. 9; grey lines). The pe pH diagram is superimposed by the respective predominance diagram for aqueous species (Fig. 9; black lines). When Np(V) sorption is weak, being controlled either by cation exchange or weak surface complexation (i.e. for $pH < 8$), reduction to Np(IV) at the surface is thermodynamically highly favored due to the strong sorption of Np(IV) even at relatively high pe. The redox boundary for the Np(V)/Np(IV) couple for illite surface bound species is by approximately 4.6 5 pe units (0.27 0.30 V) higher than for the corresponding dissolved species at $pH < 8$. For $pH > 8$, Np(V) surface complexation to illite edge sites increases, via the formation of SO NpO_2OH^- species according to the 2 SPNE SC/CE model. Consequently, reduction to Np(IV) at the illite surface becomes less favorable and the redox boundary surface species is only approximately 3 pe units (0.18 V) higher as compared to the respective solute species at $pH = 10$. Hixon et al. (2013) observed surface mediated reduction of Pu(V) to Pu(IV) in the presence of quartz. Based on the thermodynamic favorability of Pu(IV) at the quartz surface, the authors calculated that the redox potential of the Pu(V)/Pu(IV) couple would need to be raised by 0.28 V for $pH = 7$. Remarkably, although the study of Hixon et al. (2013) involves another actinide and another mineral than in this study, these independent estimations are in very good agreement.

pe pH data plotted for all experiments in Fig. 9 reveal that despite the fact that they all lie within the predominance field of aqueous Np(V) species, reduction to Np(IV) becomes thermodynamically favored in the presence of illite. In turn, we can explain the high R_d values measured under our experimental conditions due to strong sorption of Np(IV) species at the illite surface being in equilibrium with Np(V) species in solution.

The situation is somewhat different for the two samples prepared for spectroscopic studies and containing total Np concentrations as high as 3×10^{-4} M Np. Thus the amount of Np sorbed to illite exceeds the strong sites surface density (4×10^{-5} mol/L at $m/V = 20$ g/L). Based on data given in Table 1, calculations indicate partial formation of $NpO_{2(am)}$. However, sorption of Np(IV) to weak sites being present in high excess (8×10^{-4} mol/L) is also very likely. Unfortunately, data for the sorption of Np(V) and Np(IV) to illite weak sites are not available from the literature and cannot be derived from our experiments. It should be noted that weak site complexation for actinide ions is not very relevant for environmental purposes related to nuclear waste disposal. We, therefore, cannot decide at present based on available geochemical data, whether Np(IV) in those samples exists primarily as surface complex or at least partially as well as $NpO_{2(am)}$.

As mentioned before, experiments have been performed under Ar atmosphere. In absence of oxidizing or reducing agents experimentally determined pe pH values should thus follow the “redox neutral” line where $(pe + pH)=13.8$ (dashed line in Fig. 9) (Neck et al., 2007). Apparently, our data lie below this line, i.e. a reductant must be active in the system. Fe(II) is known as an efficient redox partner, inducing reduction of different elements in the presence of minerals within hours or days (Buerge and Hug, 1999; Liger et al., 1999; Nakata et al., 2002; Powell et al., 2004; Charlet et al., 2007; Chakraborty et al., 2010; Bach et al., 2014). It has been previously shown that both structural and adsorbed Fe(II) in clay systems can reduce U(VI) to U(IV) (Chakraborty et al., 2010; Latta et al., 2012). Although the illite sample investigated in our studies was purified under aerobic conditions, the presence of traces of structural Fe(II) or adsorbed Fe(II), possibly formed via partial dissolution of the clay under anaerobic conditions, cannot be ruled out. Moreover, Np(V) reduction by dissolved Fe(II) in homogeneous solution was shown to be slow (Nakata et al., 2002): only 6% of Np(IV) was formed at $pH = 4$ or 6 after one week. Therefore, a surface mediated reduction of Np(V) to Np(IV) by Fe(II) contained in the illite certainly represents one possibility. In this case reduction could be achieved by electron transfer from the bulk to the illite surface (e.g. Schaefer et al., 2011). Another option is reduction by adsorbed Fe(II) (see e.g. Chakraborty et al., 2010). A spectroscopic identification of Fe(II) in our experimental system, however, appears to be hardly possible. A maximum of 6.8×10^{-4} mol Np/kg illite was found to be reduced Np(IV). The corresponding amount of Fe(II) required for Np(V) reduction then corresponds to about 0.08% of the total amount of Fe contained in the illite (7 wt.% as Fe_2O_3 gives 0.88 mol of Fe per kg of illite). Such small fractions are very likely below the detection limit of available experimental techniques. The fact that experimental pe values are to some extent affected by the total amount of initially introduced NpO_2^+ (see Section 3.2) also suggests that the total reducing capacity in our system is low. Due to those uncertainties we are presently unable to determine precisely the nature of the redox reaction on a molecular scale. Nevertheless, the finding that sorption data can be consistently described using pe values as relevant master parameter clearly demonstrates the applicability of the thermodynamic equilibrium approach to simulate coupled redox sorption processes in clay mineral systems.

4. CONCLUSIONS

The unusually high Np(V) sorption to illite observed in the present study can be explained by partial reduction and concomitant formation of stable surface Np(IV) species. We found a clear relationship of measured pe with R_d values: Np sorption increases with decreasing redox potential. Our combined batch sorption, spectroscopic and geochemical modeling study suggests that the predominance field of reduced Np(IV) species in a pe pH diagram expands significantly due to the thermodynamically favored formation of Np(IV) surface complexes in a wide pH range. The retention of redox sensitive Np species is thus much more efficient under pe conditions only slightly below redox neutrality in presence of mineral surfaces than expected. Scoping geochemical estimations of radionuclide redox states at given pe and pH values but neglecting surface complexation reactions can thus be misleading. The result that measured pe values can be taken as a master parameter to simulate complex redox processes including surface reactions is encouraging, even though the determination of redox potentials is flawed by relatively high analytical uncertainties. Nevertheless, by using the measured pe as an input parameter, Np(IV) surface complexation constants for the 2 SPNE SC/CE model could be fitted to the experimental data which are very comparable to those values estimated by applying an established LFER approach. The complete sorption dataset can be numerically described assuming surface mediated reduction of Np(V) to Np(IV) based on the strong affinity of Np(IV) for the illite surface.

The exact mechanism of Np(V) reduction, however, could not be clarified within the present study due to the apparently limited concentration of reductant species. The fact that redox and sorption equilibria establish relatively fast, points to a surface mediated process. Electron transfer from adsorbed or structurally bound Fe(II) to surface bound Np(V) is considered a plausible mechanism for the observed coupled redox/sorption reaction. The presented modeling approach, however, predicts reduction also in absence of an explicit reductant in the solid. The thermodynamical stability of Np(IV) surface species alone is sufficient to shift the redox borderline and to induce partial Np(V) reduction.

The presented modeling concept might be applicable as well to describe the behavior of other redox sensitive elements in the geosphere.

ACKNOWLEDGEMENTS

We gratefully acknowledge Ms. Bender for laboratory work and analytical support. This work was partially financed by The Federal Ministry of Economics and Technology (Germany) under Contract No. 02E10206. The research leading to these results has received funding from the European Union's European Atomic Energy Community's (Euratom) Seventh Framework Program FP7/2007 2011 under grant agreement n° 249624 (CATCLAY project).

REFERENCES

Altmaier M., Gaona X., Fellhauer D. and Buckau G. (2010) Intercomparison of redox determination methods on designed and near neutral aqueous systems. KIT SR 7572, Karlsruhe Institute of Technology, Karlsruhe.

Altmaier M., Gaona X. and Fanghanel T. (2013) Recent advances in aqueous actinide chemistry and thermodynamics. *Chem. Rev.* **113**, 901 943.

Amayri S., Jermolajev A. and Reich T. (2011) Neptunium(V) sorption on kaolinite. *Radiochim. Acta* **99**, 349 357.

Bach D., Christiansen B. C., Schild D. and Geckeis H. (2014) TEM study of green rust sodium sulphate (GRNa, SO_4) interacted with neptunyl ions (NpO_2^+). *Radiochim. Acta* **102**(4), 279 290.

Bertrand P. A. and Choppin G. R. (1982) Separation of actinides in different oxidation states by solvent extraction. *Radiochim. Acta* **31**, 135 137.

Bradbury M. H. and Baeyens B. (2005) Experimental and modelling investigations on Na illite: Acid base behaviour and the sorption of strontium, nickel, europium and uranyl: PSI Bericht Nr. 05 02 Paul Scherrer Institut, Villigen, Switzerland and Nagra NTB 04 02, Nagra, Wettingen, Switzerland.

Bradbury M. H. and Baeyens B. (2006) Modelling sorption data for the actinides Am(III), Np(V) and Pa(V) on montmorillonite. *Radiochim. Acta* **94**, 619 625.

Bradbury M. H. and Baeyens B. (2009a) Sorption modelling on illite Part I: Titration measurements and the sorption of Ni Co, Eu and Sn. *Geochim. Cosmochim. Acta* **73**, 990 1003.

Bradbury M. H. and Baeyens B. (2009b) Sorption modeling on illite Part II: Actinide sorption and linear free energy relationships. *Geochim. Cosmochim. Acta* **73**, 1004 1013.

Brendebach B., Banik N. L., Marquardt C. M., Rothe J., Denecke M. and Geckeis H. (2009) X ray absorption spectroscopic study of trivalent and tetravalent actinides in solution at varying pH value. *Radiochim. Acta* **97**, 701 708.

Buerge I. J. and Hug S. J. (1999) Influence of mineral surfaces on chromium(VI) reduction by iron(II). *Environ. Sci. Technol.* **33**, 4285 4291.

Chakraborty S., Favre F., Banerjee D., Scheinost A. C., Mullet M., Ehrhardt J. J., Brendle J., Vidal L. and Charlet L. (2010) U(VI) sorption and reduction by Fe(II) sorbed on montmorillonite. *Environ. Sci. Technol.* **44**(10), 3779 3785.

Charlet L., Scheinost A. C., Tournassat C., Greneche J. M., Géhin A., Fernandez Martinez A., Coudert S., Tisserand D. and Brendle J. (2007) Electron transfer at the mineral/water interface. Selenium reduction by ferrous iron sorbed on clay. *Geochim. Cosmochim. Acta* **71**, 5731 5749.

Claret F., Schafer T., Rabung T., Wolf M., Bauer A. and Buckau G. (2005) Differences in properties and Cm(III) complexation behavior of isolated humic and fulvic acid derived from Opalinus clay and Callovo Oxfordian argillite. *Appl. Geochem.* **20**, 1158 1168.

Degueldre C. and Bolek M. (2009) Modelling colloid association with plutonium: The effect of pH and redox potential. *Appl. Geochem.* **24**, 310 318.

Denecke M. A., Dardenne K. and Marquardt C. M. (2005) Np(IV)/Np(V) valence determinations from Np L3 edge XANES/EXAFS. *Talanta* **65**, 1008 1014.

Freundlich H. (1909) *Kapillarchemie*. AkademischeVerlagsgesellschaft, Leipzig, Germany.

Frohlich D. R., Amayri S., Drebert J. and Reich T. (2011) Sorption of neptunium(V) on Opalinus Clay under aerobic/anaerobic conditions. *Radiochim. Acta* **99**, 71 77.

Frohlich D. R., Amayri S., Drebert J., Grolimund D., Huth J., Kaplan U., Krause J. and Reich T. (2012) Speciation of Np(V) uptake by Opalinus Clay using synchrotron microbeam techniques. *Anal. Bioanal. Chem.* **404**, 2151 2162.

Gabis V. (1963) Etude mineralogique et geochimique de la seriesedimentaireoligocene du Velay. *Bulletin Societe Francaise de Mineralogie et Cristallographie* **86**, 315 354.

Gaona X., Tits J., Dardenne K., Liu X., Rothe J., Denecke M. A., Wieland E. and Altmaier M. (2012) Spectroscopic investigations of Np(V/VI) redox speciation in hyperalkaline TMA (OH, Cl) solutions. *Radiochim. Acta* **100**, 759 770.

Geckeis H., Lutzenkirchen J., Polly R., Rabung T. and Schmidt M. (2013) Mineral water interface reactions of actinides. *Chem. Rev.* **13**(2), 1016 1062.

Gorgeon L. (1994) Contribution à la modélisation physico chimique de la rétention de radioéléments à vie longue par des matériaux argileux. Ph.D. thesis, Université Paris 6.

Guillaumont R., Fanghanel Th., Fuger J., Grenthe I., Neck V., Palmer D. A. and Rand M. H. (2003) Update on the chemical thermodynamics of uranium, neptunium, plutonium, americium and technetium. In *Chemical Thermodynamics*, vol. 5 (eds. F. J. Mompean, C. Domenech Orti, K. Ben Said and OECD/NEA Data Bank). Elsevier, Amsterdam.

Hixon A. E., Hu Y. J., Kaplan D. I., Kukkadapu R. K., Nitsche H., Qafoku O. and Powell B. A. (2010) Influence of iron redox transformations on plutonium sorption to sediments. *Radiochim. Acta* **98**, 685 692.

Hixon A. E., Arai Y. and Powell B. A. (2013) Examination of the effect of alpha radiolysis on plutonium(V) sorption to quartz using multiple plutonium isotopes. *J. Colloid. Int. Sci.* **403**, 105 112.

Kim J. I. (1986) Chemical behaviour of transuranic elements in natural aquatic systems. In *Handbook on the Physics and Chemistry of the Actinides* (ed. A. J. Freeman). Elsevier Science Publishers B.V., Amsterdam, p. 413.

Kinniburgh D. G. and Cooper D. M. (2009) PhreePlot: Creating graphical output with PHREEQC. <http://www.phreeplot.org.

Kirsch R., Fellhouer D., Altmaier M., Neck V., Rossberg A., Fanghanel T., Charlet L. and Scheinost A. C. (2011) Oxidation state and local structure of plutonium reacted with magnetite, mackinawite, and chukanovite. *Environ. Sci. Technol.* **45**, 7267 7274.

Latrille C., Ly J. and Herbette M. (2006) Retention of Sn(IV) and Pu(IV) onto four argillites from the Callovo Oxfordian level at Bure (France) from eight equilibrated sedimentary waters. *Radiochim. Acta* **94**, 421 427.

Latta D. E., Boyanov M. I., Kemner K. M., O'Loughlin E. J. and Scherer M. M. (2012) Abiotic reduction of uranium by Fe(II) in soil. *Appl. Geochem.* **27**, 1512 1524.

Liger L., Charlet L. and Van Cappellen P. (1999) Surface catalysis of uranium(VI) reduction by iron(II). *Geochim. Cosmochim. Acta* **63**, 2939 2955.

Marques Fernandes M., Baeyens B., Dahn R., Scheinost A. C. and Bradbury M. H. (2012) U(VI) sorption on montmorillonite in the absence and presence of carbonate: A macroscopic and microscopic study. *Geochim. Cosmochim. Acta* **93**, 262 277.

Nakata K., Nagasaki S., Tanaka S., Sakamoto Y., Tanaka and Ogawa H. (2002) Sorption and reduction of neptunium(V) on the surface of iron oxides. *Radiochim. Acta* **90**, 665 669.

Neck V., Altmaier M. and Fanghanel T. (2007) Solubility of plutonium hydroxides/hydrous oxides under reducing conditions and in the presence of oxygen. *C. R. Chimie* **10**, 959 977.

Nitsche H., Lee S. C. and Gatti R. C. (1988) Determination of plutonium oxidation states at trace levels pertinent to nuclear waste disposal. *J. Radioanal. Nucl. Chem.* **124**, 171 185.

Nitsche H., Roberts K., Xi R., Prussin T., Becraft K., Mahamid I. A., Silber H. B., Carpenter S. A. and Gatti R. C. (1994) Long term plutonium solubility and speciation studies in a synthetic brine. *Radiochim. Acta* **66**, 3 7.

Parkhurst D. L. and Appelo C. A. J. (1999) User's guide to PHREEQC (Version 2) a computer program for speciation, batch reaction, one dimensional transport and inverse geochemical calculation. Water resources Investigation Report 99 4259, USGS, Denver, Colorado, p. 312.

Poinssot C., Baeyens B. and Bradbury M. H. (1999). Experimental studies of Cs, Sr, Ni and Eu sorption on Na illite and the modelling of Cs sorption. PSI Bericht Nr. 99 06. Paul ScherrerInstitut, Villigen and Nagra Technical Report NTB 99 04, Nagra, Wettingen, Switzerland.

Powell M. J. D. (1965) A method for minimizing a sum of squares of non linear functions without calculating derivatives. *The Computer Journal* **7**, 303 307.

Powell B. A., Fjeld R. A., Kaplan D. I., Coates J. T. and Serkiz S. M. (2004) Pu(V)O_2^+ adsorption and reduction by synthetic magnetite (Fe_3O_4). *Environ. Sci. Technol.* **38**, 6016.

Powell B. A., Fjeld R. A., Kaplan D. I., Coates J. T. and Serkiz S. M. (2005) Pu(V)O_2^+ adsorption and reduction by synthetic hematite and goethite. *Environ. Sci. Technol.* **39**, 2107.

Ravel B. and Newville M. (2005) ATHENA and ARTEMIS: Data analysis for X ray absorption spectroscopy using IFEFFIT. *Journal of Synchrotron Radiation* **12**, 537 541.

Rothe J., Denecke M. A., Dardenne K. and Fanghanel T. (2006) The INE Beamline for actinide research at ANKA. *Radiochim. Acta* **94**, 691.

Rothe J., Butorin S., Dardenne K., Denecke M. A., Kienzler B., Loble M., Metz V., Seibert A., Steppert M., Vitova T., Walther C. and Geckeis H. (2012) The INE Beamline for actinide science at ANKA. *Rev. Sci. Instrum.* **83**, 043105.

Schaefer M., Gorski C. A. and Scherer M. M. (2011) Spectroscopic evidence for interfacial Fe(II) Fe(III) electron transfer in a clay mineral. *Environ. Sci. Technol.* **45**, 540 545.

Schuring J., Schulz H. D., Fischer W. R., Bottcher J. and Duijnisveld W. H. M. (2000) *Redox: Fundamentals, Processes and Applications*. Springer Verlag, Berlin, Heidelberg, New York, 251 p.

Schwantes J. M. and Santschi P. H. (2010) Mechanisms of plutonium sorption to mineral oxide surfaces: New insights with implications for colloid enhanced migration. *Radiochim. Acta* **98**, 737 742.

Sjoblom R. and Hindman J. C. (1951) Spectrophotometry of neptunium in perchloric acid solutions. *J. Am. Chem. Soc.* **73**(4), 1744 1751.

Stumm W. (1992) *Chemistry of the Solid water Interface*. Wiley Interscience, New York.

Turner D. R., Pabalan R. T. and Bertetti F. P. (1998) Neptunium(V) sorption on montmorillonite: An experimental and surface complexation modeling study. *Clays Clay Miner.* **46**, 256.

Wu T., Amayri S., Drebert J., Van Loon L. R. and Reich T. (2009) Neptunium(V) sorption and diffusion in Opalinus clay. *Environ. Sci. Technol.* **43**, 6567 6571.

Zaravin M., Powell B. A., Bourbin M., Pihong Zhao P. and Kersting A. B. (2012) NpO_2^+ and Pu(V) ion exchange and surface mediated reduction mechanisms on montmorillonite. *Environ. Sci. Technol.* **46**, 2692 2698.

Associate editor: Annie B. Kersting

Marsac, R.; Banik, N. I.; Lützenkirchen, J.; Marquardt, C. M.; Dardenne, K.; Schild, D.; Roth, J.; Diascorn, A.; Kupcik, T.; Schäfer, T.; Geckeis, H.
Neptunium redox speciation at the illite surface
2015. Geochimica et cosmochimica acta, 152
doi: 10.554/IR/110099923

Marsac, R.; Banik, N. I.; Lützenkirchen, J.; Marquardt, C. M.; Dardenne, K.; Schild, D.; Roth, J.; Diascorn, A.; Kupcik, T.; Schäfer, T.; Geckeis, H.
Neptunium redox speciation at the illite surface
2015. Geochimica et cosmochimica acta, 152, 39–51.
doi:10.1016/j.gca.2014.12.021